PAPER

Check for updates

Improved performance of all-solution-processed quantum dot light-emitting diodes with TFB/PVK double-hole transport layers using 1,2-dichloroethane†

Jaeyeop Lee,‡[a] Woon Ho Jung,‡[b] Kyoungeun Lee,[a] Yeyun Bae,[a] Minseok Choi,[a] Jiyoon Oh,[ae] Jaehoon Lim [ID] [bcd] and Jeongkyun Roh [ID] *[a]

High-performance quantum dot light-emitting diodes (QD-LEDs) require balanced electron and hole injection into the QD emissive layer—an especially difficult task when using all-solution processes. One effective strategy for achieving this balance is to create a stepwise hole injection pathway *via* double-hole transport layers (D-HTLs). Poly(9-vinylcarbazole) (PVK) and poly[(9,9-dioctylfluorenyl-2,7-diyl)-*co*-(4,4′-(*N*-(4-*sec*-butylphenyl)diphenylamine)]) (TFB) are commonly employed in D-HTLs because of their favorable energy level alignment and suitable hole mobilities. However, constructing TFB/PVK D-HTLs demands careful attention to solvent orthogonality, as both polymers often dissolve in the same solvent. Thus, identifying a solvent system that enables the formation of TFB/PVK D-HTLs without damaging the TFB layer is crucial. In this study, we systematically investigate the solvent orthogonality of TFB/PVK and demonstrate high-performance QD-LEDs fabricated entirely by solution processes. We examine various PVK solvents—evaluating their polarity, solubility, and potential to damage the TFB layer—and identify 1,2-dichloroethane (1,2-DCE) as optimal for forming TFB/PVK D-HTLs with minimal damage. The resulting all-solution-processed QD-LEDs exhibit a 1.5-fold increase in external quantum efficiency compared to devices employing a single HTL. Furthermore, 1,2-DCE also proves effective in inverted QD-LED architectures, protecting the QD emissive layer during PVK deposition and demonstrating its versatility across multiple device architectures.

1. Introduction

Colloidal quantum dots (QDs) hold great promise for display applications due to their tunable emission wavelengths, high photoluminescence quantum yield (PLQY), and narrow full width at half maximum (FWHM).[1–6] These favorable characteristics have led to intensive research on electroluminescent devices, particularly QD light-emitting diodes (QD-LEDs). Since the first demonstration of QD-LEDs by Colvin *et al.*,[7] device

[a]Department of Electrical Engineering, Pusan National University, 2 Busandaehak-ro 63 beon-gil, Geumjeong-gu, Busan 46241, Republic of Korea. E-mail: jkroh@pusan.ac.kr

[b]Department of Energy Science, Center for Artificial Atoms, Sungkyunkwan University (SKKU), Suwon, Gyeonggi-do 16419, Republic of Korea

[c]SKKU Institute of Energy Science and Technology (SIEST), Sungkyunkwan University, Suwon, Gyeonggi-do 16419, Republic of Korea

[d]Department of Future Energy Engineering (DFEE), Sungkyunkwan University, Suwon, Gyeonggi-do 16419, Republic of Korea

[e]Extreme Process Control Group, Korea Institute of Industrial Technology (KITECH), Busan 46938, Republic of Korea

† Electronic supplementary information (ESI) available. See DOI: https://doi.org/10.1039/d5na00120j

‡ Jaeyeop Lee and Woon Ho Jung contributed equally to this work.

performance has improved markedly, propelled by advances in luminescent QDs and optimized device architectures.[8–12] State-of-the-art QD-LEDs typically employ a hybrid charge-transport layer that combines an organic hole transport layer (HTL) with a zinc oxide (ZnO)-based inorganic electron transport layer (ETL).[9,11,13] However, in this architecture, the electron injection rate from ZnO ETLs often exceeds the hole injection rate from organic HTLs, leading to an imbalance in carrier injection into the QD emissive layer (EML). This causes nonradiative Auger recombination, which significantly reduces QD-LED luminescence efficiency.[14] Consequently, achieving balanced electron and hole injection into the QD EML is essential for high-performance QD-LEDs. Various strategies, including interlayers or doping, have been proposed to either suppress electron injection or enhance hole injection into the QD EML.[15–17] Nonetheless, achieving balanced injection rates into the QD EML of all-solution-processed QD-LEDs remains challenging.

To capitalize on the advantages of colloidal QDs—such as low fabrication costs and large-area processability—nearly all device layers (except electrodes) must be deposited from solution. Unfortunately, the limited selection of solution-processable materials and challenges in depositing multiple layers without

dissolving underlying films complicate the task of achieving optimal charge balance within the QD EML of all-solution-processed QD-LEDs. One promising route is to enhance hole injection into QD EMLs by incorporating double HTLs (D-HTLs).[18,19] This approach typically utilizes two widely used solution-processable HTLs: poly[(9,9-dioctylfluorenyl-2,7-diyl)-co-(4,4'-(N-(4-sec-butylphenyl)diphenylamine))] (TFB) and poly(9-vinylcarbazole) (PVK). These two materials establish a stepwise injection pathway for holes from the anode to the QDs, improving charge injection balance into QD EMLs. Moreover, the D-HTL design capitalizes on each material's advantages: TFB's relatively high hole mobility and PVK's lower energy-level offset with QDs.[18,20–22] Nonetheless, because both TFB and PVK are soluble in many commonly used organic solvents, fabricating D-HTLs without damaging the underlying layers can be difficult. While crosslinking the bottom HTL is one viable strategy to mitigate this issue, it often requires additional synthetic steps or cross-linking agents.[23,24] In contrast, employing solvent-orthogonality strategies provides a more direct way to protect the underlying layer and is considered simpler for solution-processed QD-LEDs. Although solvents such as 1,4-dioxane (1,4-DO) have been used for PVK to minimize the dissolution of TFB, significant erosion of the TFB layer can still occur during PVK deposition.[19,25,26] Hence, identifying a more suitable solvent system to construct D-HTLs is crucial for realizing high-performance all-solution-processed QD-LEDs.

In this study, we systematically investigate solvent orthogonality for TFB/PVK-based D-HTLs and demonstrate significantly improved performance in all-solution-processed QD-LEDs. Our findings show that 1,2-dichloroethane (1,2-DCE) is a suitable PVK solvent in constructing TFB/PVK D-HTLs, offering sufficient solubility and higher polarity compared to the commonly used 1,4-DO—thereby reducing the dissolution rate of the underlying TFB layer. Through absorption spectroscopy and atomic force microscopy (AFM), we confirm the solvent orthogonality of 1,2-DCE on TFB films, enabling the successful fabrication of TFB/PVK D-HTLs without eroding the TFB layer. By enhancing hole injection and improving charge balance within the QD EML through D-HTLs, the all-solution-processed QD-LED exhibits markedly improved performance, with the maximum luminance increasing from 87 779 cd m^{-2} to 111 572 cd m^{-2} and the maximum external quantum efficiency rising from 9.2% to 13.7%—a 1.5-fold improvement over devices employing a single HTL (S-HTL). These results indicate the effectiveness of D-HTLs fabricated with 1,2-DCE for boosting the performance of all-solution-processed QD-LEDs.

2. Experimental section

2.1. Materials

Patterned indium tin oxide (ITO) substrates were purchased from AMG. The TFB polymer was purchased from OSM. Poly(9-vinylcarbazole) (PVK) polymer, ethanol (≥99.5%), zinc acetate dihydrate (≥99.0%), ethanolamine (≥99.5%), zinc acetate (99.999%), selenium powder (200 mesh, 99.999), sulfur powder (99.98%), and octane (≥99%) were obtained from Sigma-Aldrich. Oleic acid (OA, 90%), trioctylphosphine (TOP, 97%), 1-octadecene (ODE, 99%), cadmium oxide (CdO, 99.95%),

myristic acid (My, 99%), and 1-dodecanethiol (DDT, 98%) were purchased from Alfa Aesar. PEDOT:PSS Clevios P VP AI 4083 was sourced from the Heraeus Electronic Materials division, and aluminum (Al) pellets were purchased from iTASCO. Potassium hydroxide (KOH), methanol (≥99.9%), isopropyl alcohol (IPA) (≥99.9%), and acetone (≥99.7%) were purchased from Sam-chun Chemicals. All chemicals were used as received without further purification.

2.2. Synthesis of ZnO NPs

ZnO nanoparticles (NPs) were synthesized by reacting zinc acetate dihydrate with KOH in a methanol solution for 2 h and 30 min. Initially, zinc acetate dihydrate (5.0 g) was dissolved in 200 mL of methanol with 0.8 mL of deionized water and then stirred for 30 min. The KOH solution (2.5 g in 50 mL of methanol) was added to the zinc acetate dihydrate solution and stirred continuously for 2 h and 30 min. The ZnO NPs were purified by washing twice with methanol and n-hexane, followed by centrifugation. Ethanolamine ligand treatment was applied to the purified ZnO NPs, and then the ZnO NPs were dissolved in pure ethanol for subsequent use.

2.3. Synthesis of QDs

Red-emitting CdSe/CdS/CdZnS QDs were synthesized based on a method reported by Lisa zur Borg et al.,[27] with slight modifications. In an inert atmosphere, zinc oleate (Zn(OA)$_2$), cadmium oleate (Cd(OA)$_2$), TOP-Se, and TOP-S precursors were prepared. For Zn(OA)$_2$, 20 mmol of zinc acetate, 20 mL of 1-ODE, and 20 mL of OA were mixed in a 100 mL three-neck flask. The mixture was degassed at 120 °C before switching to an N$_2$ environment and heating to 300 °C. The preparation of Cd(OA)$_2$ followed the same approach, except that the temperature was raised to 270 °C after degassing. The formation of the oleate solutions was confirmed by their transition from turbid to an optically clear state. Both oleate solutions were kept at 120 °C in preparation for the QD synthesis. For TOP-Se and TOP-S, 2 M solutions were prepared using elemental selenium and sulfur, respectively.

The CdSe/CdS/CdZnS QDs were synthesized using a one-pot multi-injectional method. To form the CdSe core, 1 mmol of CdO, 3 mmol of My, and 15 mL of 1-ODE were mixed in a three-neck flask. The mixture was degassed at 120 °C, exchanged to an N$_2$ environment, and heated to 270 °C until the solution became optically clear. At this stage, 0.5 mmol of TOP-Se was injected and allowed to react for 3 min to form the CdSe core. Subsequently, 1.5 mmol of DDT and 1 mmol of Zn(OA)$_2$ were added as the temperature increased to 300 °C, and the reaction continued for 30 min.

For the CdZnS shell growth, an initial injection of 2 mmol of Zn(OA)$_2$ and 3 mmol of TOP-S, followed by 2 mmol of Cd(OA)$_2$, was performed for 1 min, with the reaction maintained for 9 min. An additional CdZnS shell growth included injecting 3 mmol Zn(OA)$_2$, 4 mmol TOP-S, and 1.5 mmol Cd(OA)$_2$ for 1 min, followed by a 5-min reaction before quenching to room temperature. The synthesized CdSe/CdS/CdZnS QDs were purified with

acetone and toluene, repeating the purification process four more times. The purified QDs were then dispersed in octane.

2.4. Fabrication of QD-LEDs

The ITO-patterned substrates were cleaned in an ultrasonic bath with acetone, IPA, and deionized water for 20 min and then dried in an oven at 100 °C. After a 15-min UV ozone treatment, PEDOT:PSS (filtered through a 0.45 μm ADVANTEC filter) was spin-coated onto the ITO substrates at 3000 rpm for 45 s and baked at 150 °C for 15 min. The substrates with PEDOT: PSS were transferred to a nitrogen-filled glove box for subsequent layer deposition. The first HTL of TFB (8 mg mL^{-1}) was spin-coated at 4000 rpm for 30 s and baked at 150 °C for 25 min. Next, the second HTL of PVK (2 mg mL^{-1}) was spin-coated at 4000 rpm for 45 s and baked at 100 °C for 25 min. The red QDs (CdSe/CdS/CdZnS capped with OA and DDT, 14 mg mL^{-1} in n-octane) were then spin-coated at 4000 rpm for 45 s and baked at 90 °C for 15 min. ZnO NPs as an ETL (20 mg mL^{-1} in ethanol) were then spin-coated at 2000 rpm for 60 s and baked at 90 °C for 30 min. Finally, the substrates were transferred to a high-vacuum thermal evaporator for Al cathode deposition at a pressure below 1.0×10^{-6} torr. The active area of the devices was controlled to be 1.96 mm^2 using a fine metal mask. All devices were encapsulated with a commercially available UV-curing resin and cover glass.

2.5. Characterization of QD-LEDs

The current density–voltage–luminance (J–V–L) characteristics of the QD-LEDs were measured using a Keithley 2450 source meter and Konica Minolta CS-2000 spectroradiometer. Absorption spectra were obtained with a V-770 UV-visible and NIR spectrometer (JASCO Instruments Inc.). Surface morphology measurements were performed using an NX10 atomic force microscope (Park Systems).

3. Results and discussion

To determine an ideal solvent for fabricating the D-HTLs, we investigated the solubility of TFB and PVK in various solvents, focusing on finding a solvent that adequately dissolves PVK

well, while exerting minimal impact on TFB. PVK's chemical structure features a carbazole group, which introduces polarity through the nitrogen atom in the carbazole ring. This polarity facilitates strong dipole–dipole interactions with polar solvents, thereby increasing PVK's solubility in such environments.[28] In contrast to PVK, which contains a backbone composed solely of carbazole units, TFB incorporates both triphenylamine and carbazole units in its backbone. Moreover, TFB's structure includes long alkyl side chains attached to a fluorene backbone, rendering it primarily nonpolar. This reduces TFB's interactions with polar solvents, leading to limited solubility. Consequently, PVK exhibits greater solubility in polar solvents than TFB.

Potential solvents for constructing TFB/PVK D-HTLs were selected based on their relative polarity, and we tested the solubility of TFB and PVK at a concentration of 8 mg mL^{-1}. The tested solvents included acetone, IPA, octane, m-xylene, toluene, chlorobenzene, 1,4-DO, and 1,2-DCE. Given that 1,4-DO is commonly used in TFB/PVK D-HTL fabrication, we selected 1,4-DO as a reference solvent. Fig. 1(a) presents the solutions of TFB (top) and PVK (bottom) in these solvents. Our observation confirmed that TFB did not dissolve in highly polar or nonpolar solvents, such as acetone, IPA, and octane (Fig. 1(a), top). Likewise, these solvents were also unsuitable for PVK, as PVK failed to dissolve in them (Fig. 1(a), bottom). Some solvents, including m-xylene, toluene, and chlorobenzene (CB), dissolved both TFB and PVK, indicating they are unsuitable for TFB/PVK D-HTLs. By contrast, 1,4-DO and 1,2-DCE dissolved PVK but had limited solubility for TFB, suggesting their suitability for this application. In particular, 1,2-DCE exhibited excellent solubility for PVK while maintaining low solubility for TFB, making it a promising candidate. Additionally, PVK dissolved more efficiently in 1,2-DCE than in 1,4-DO, as confirmed by our tests, while TFB showed minimal dissolution in 1,2-DCE.

To further confirm the suitability of 1,2-DCE for constructing TFB/PVK D-HTLs, we conducted a solvent-rinsing test. Solvents were spin-coated at 4000 rpm for 45 s onto TFB thin films on glass substrates, and the absorption spectra of the rinsed TFB films were subsequently measured using UV-visible and NIR spectrometers (Fig. 1(b) and S1†). As expected, the absorption spectrum of the TFB films completely vanished after rinsing with CB, indicating significant dissolution of the film.
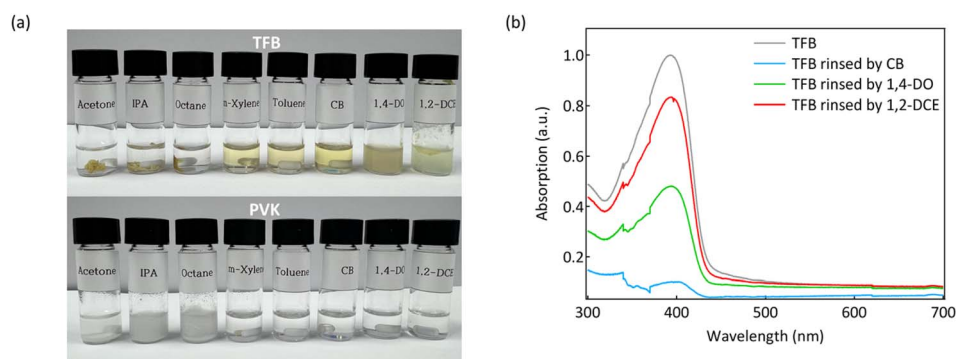

Fig. 1 (a) Photographs of TFB and PVK in different solvents. The solvents from left to right are acetone, IPA, octane, m-xylene, toluene, chlorobenzene (CB), 1,4-dioxane (1,4-DO), and 1,2-dichloroethane (1,2-DCE). (b) Absorption spectra of TFB films with and without rinsing with different solvents.
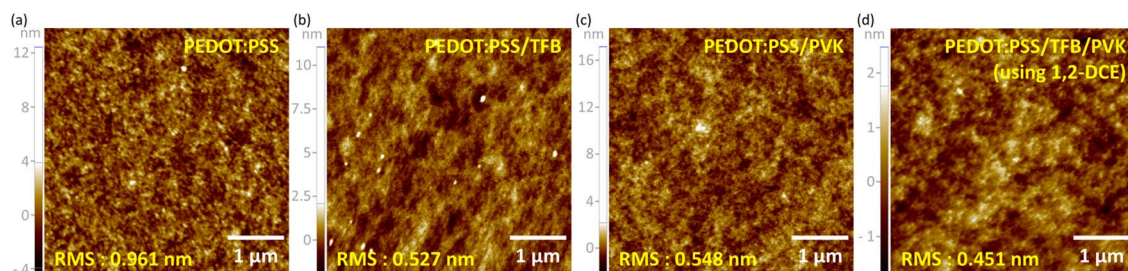
Fig. 2 AFM images (5 μm × 5 μm) of (a) PEDOT:PSS, (b) PEDOT:PSS/TFB, (c) PEDOT:PSS/PVK, and (d) PEDOT:PSS/TFB/PVK using 1,2–DCE as the PVK solvent.

Conversely, the peak positions in the TFB absorption spectra remained consistent for samples rinsed with both 1,2-DCE and 1,4-DO. Nevertheless, the sample rinsed with 1,2-DCE exhibited higher absorption intensity than the one rinsed with 1,4-DO. Thus, 1,2-DCE minimizes damage to the underlying TFB layer more effectively than 1,4-DO. These findings suggest that 1,2-DCE is a superior solvent for constructing TFB/PVK D-HTLs.

Stacking thin films using solution processing can lead to non-uniform surface morphology caused by erosion effects. A rough surface may create interfacial defects, ultimately degrading the performance of QD-LEDs.[29] Therefore, achieving a smooth surface morphology in each layer of all-solution-processed QD-LEDs is crucial for attaining high performance and stability. To evaluate the thin-film morphologies of these solution-processed D-HTLs, we conducted AFM measurements (Fig. 2 and S2†). The root mean square (RMS) roughness values were as follows: 0.961 nm for PEDOT:PSS, 0.527 nm for PEDOT:PSS/TFB, 0.548 nm for PEDOT:PSS/PVK, and 0.644 nm for PEDOT:PSS/TFB/PVK using 1,4-DO as a PVK solvent, and 0.451 nm for PEDOT:PSS/TFB/PVK using 1,2-DCE as PVK solvent. Generally, the PEDOT:PSS hole injection layer (HIL) remains undamaged by subsequent organic HTL depositions because of solvent orthogonality, thereby allowing smooth TFB and PVK films to form on PEDOT:PSS, as indicated by the reduced RMS roughness values. The surface roughness of the TFB/PVK D-HTLs fabricated with 1,2-DCE is similar to that of the S-HTL films, indicating that D-HTL fabrication with 1,2-DCE does not significantly erode the underlying layer. Thus, this 1,2-DCE-fabricated TFB/PVK D-HTL structure does not introduce

additional interfacial defects associated with surface morphology,[29] which is advantageous for QD-LED fabrication.

Subsequently, we fabricated hole-only devices (HODs) incorporating TFB/PVK D-HTLs to confirm enhanced hole injection into the QD EML using D-HTLs processed with 1,2-DCE. Fig. 3(a) presents the energy band diagram of these HODs. They were designed to suppress electron contribution to the total current by creating a substantial electron injection barrier, ensuring that the current primarily reflects hole injection and transport capabilities. The HODs were structured as ITO/PEDOT:PSS/S-HTL or D-HTLs/QDs/TCTA/MoO$_x$/Al. Before fabricating the HODs, we measured the thicknesses of the single-layer TFB and PVK films by AFM, confirming thicknesses of approximately 28 nm and 22 nm, respectively. For the double-layer TFB/PVK stack using 1,2-DCE, an AFM step-height measurement (Fig. S3†) showed a slightly greater total thickness (31 nm) than the single TFB layer. The logarithmic J–V plot of HODs in Fig. 3(b) reveals that HODs employing TFB as the S-HTL exhibited a higher current density (J) than those with PVK, consistent with the superior hole mobility of TFB ($\mu_h \sim 10^{-3}$ cm^2 V^{-1} s^{-1})[30] compared to PVK ($\mu_h \sim 10^{-6}$ cm^2 V^{-1} s^{-1}).[31] The HODs featuring D-HTLs exhibited higher current densities owing to the enhanced hole injection efficiency enabled by a stepwise injection pathway that reduces the carrier injection barrier. Further analysis of carrier injection efficiency was conducted by fitting the HOD J–V curves using the power law $J \propto V^n$.[21,26,32–34] (Fig. 3(c)).

The J–V characteristics of the HODs revealed two conduction regions distinguished by the exponent n: an ohmic conduction region with $n \approx 1$ and a trap-limited conduction region where n
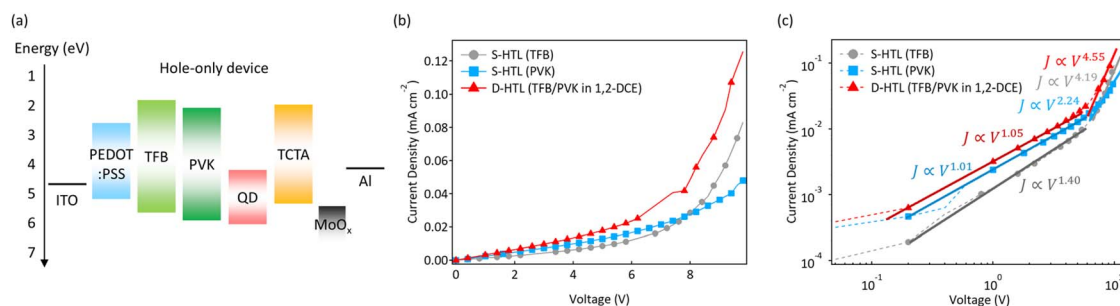

Fig. 3 Characteristics of hole-only devices (HODs). (a) Energy band diagram of HODs with the variation of HTLs, and (b) linear and (c) logarithmic plots of current–voltage characteristics of HODs with fitting lines based on the power law, $J \propto V^n$.
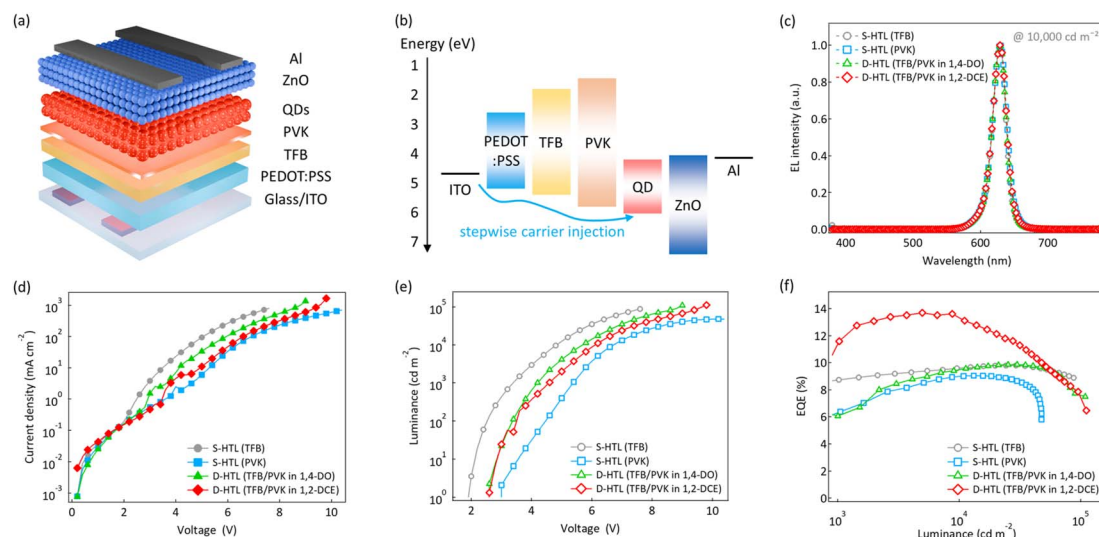
Fig. 4 Schematic illustration of (a) the device structure and (b) the energy band diagram for QD-LEDs incorporating TFB/PVK D-HTLs. (c–f) The performance of QD-LEDs using TFB/PVK D-HTLs processed with either 1,2-DCE and 1,4-DO, compared with the devices featuring an S-HTL (TFB or PVK): (c) normalized EL spectrum, (d) current density–voltage characteristics, (e) luminance–voltage characteristics, and (f) external quantum efficiency–luminance characteristics.

> 2. The injection efficiency of the devices is assessed based on the exponent in the trap-limited conduction region, where a higher exponent indicates better charge transport.[34] In the ohmic region ($n \approx 1$), the observed n values were approximately 1.40 for TFB, 1.01 for PVK, and 1.05 for TFB/PVK D-HTLs. In the trap-limited conduction region ($n > 2$), the n values were 4.18 for TFB, 2.24 for PVK, and 4.55 for TFB/PVK D-HTLs. The lower n value observed in PVK-based HODs can be attributed to the injection barrier at the PEDOT:PSS/PVK interface, as PVK has a deep-lying highest occupied molecular orbital (HOMO) level.[35] The TFB-based HOD exhibited a higher n exponent than PVK but remained lower than the TFB/PVK D-HTL device due to the notable injection barrier between TFB and QDs. These results reaffirm that D-HTLs improve hole injection efficiency compared to S-HTLs by providing a more gradual energy landscape for holes, thus reducing the hole injection barrier.[34,36]

Finally, we fabricated all-solution-processed QD-LEDs incorporating D-HTLs. The QD-LEDs consisted of ITO (150 nm)/PEDOT:PSS (40 nm)/S-HTL or D-HTLs (S-HTL (TFB): 28 nm, S-HTL (PVK): 22 nm, D-HTL (using 1,4-DO): 16.5 nm, D-HTLs (using 1,2-DCE): 31 nm)/QDs (25 nm)/ZnO (33 nm)/Al (100 nm)

(Fig. 4(a)). Fig. 4(b) depicts the energy band diagram of QD-LEDs with TFB/PVK D-HTLs, illustrating a smooth hole injection pathway and improved electron confinement within the QD EML due to the electron-blocking properties of PVK. The electroluminescence (EL) spectra of QD-LEDs employing either S-HTLs or D-HTLs (Fig. 4(c)) showed a maximum EL peak at 629 nm with a full width at half maximum (FWHM) of 24 nm, exhibiting no notable parasitic emission. Fig. 4(d and e) present the current density–voltage (J–V) and luminance–voltage (L–V) characteristics of the QD-LEDs, respectively. The QD-LED incorporating the D-HTLs exhibited a turn-on voltage (V_{on})—defined as the voltage at which the luminance reaches 1 cd m^{-2}—lying between those of the TFB and PVK-based S-HTL devices. Importantly, QD-LEDs with D-HTLs exhibited higher maximum luminance, suggesting improved device stability originating from enhanced charge balance in the QD EML. In particular, QD-LEDs with 1,2-DCE-based D-HTLs achieved the highest maximum luminance (L_{max}) of 111 572 cd m^{-2} at an applied voltage of 9.8 V. Fig. 4(f) shows the external quantum efficiency–current density (EQE–J) characteristics, revealing that QD-LEDs incorporating 1,2-DCE-based D-HTLs attained the highest EQE of 13.7%, which is 1.5 times

Table 1 EL performance of the QD-LEDs with different HTLs

			TFB/PVK	
	TFB S-HTL	PVK S-HTL	D-HTLs (1,4-DO)	D-HTLs (1,2-DCE)
V_{on}[a] [V]	1.8	2.9	2.5	2.5
L_{max}[b] [cd m^{-2}]	87 779	47 769	109 143	111 572
EQE$_{max}$[c] [%]	9.2	9.0	9.9	13.7
EL peak[d] [nm]	629	629	629	629
FWHM[e] [nm]	24	24	24	24

[a] Turn-on voltage at 1 cd m^{-2} [b] Maximum luminance. [c] Maximum external quantum efficiency. [d] Electroluminescence peak at 8 V. [e] Full width at half maximum.

greater than that of the devices with the TFB S-HTL (EQE of 9.2%). This superior EQE, compared to D-HTL devices fabricated with 1,4-DO (EQE of 9.9%), is attributed to the partial dissolution of the TFB layer by 1,4-DO during PVK deposition, highlighting the suitability of 1,2-DCE for constructing TFB/PVK D-HTLs. Furthermore, QD-LEDs incorporating 1,2-DCE-based D-HTLs exhibit stable efficiency roll-off, maintaining more than 70% of their peak EQE over a wide luminance range (from 4981.2 cd m^{-2} to 56 609 cd m^{-2}). This performance represents a considerable improvement compared to the PVK S-HTL device, which retains more than 70% of its peak EQE only within a much narrower luminance window (from 13 194 cd m^{-2} to 47 376 cd m^{-2}) (Fig. S4†). Table 1 summarizes the performance of QD-LEDs with different HTLs.

We also performed EL lifetime measurements on QD-LEDs at an initial luminance of 10 000 cd m^{-2} (Fig. S5†), revealing significant improvements in devices utilizing 1,2-DCE-based D-HTLs. Unlike the rapid luminance decay observed for S-HTL devices, where the T_{50} lifetimes were 2.44 hours for TFB and 1.95 hours for PVK, QD-LEDs incorporating 1,2-DCE-based D-HTLs retained their luminance over an extended period, exhibiting a more gradual decline. Specifically, devices with 1,2-DCE-based D-HTLs achieved a T_{50} lifetime of 5.35 hours, which is considerably longer than the 3.60 hours observed for those using 1,4-DO-based D-HTLs, highlighting the benefits of using 1,2-DCE to construct TFB/PVK D-HTLs.

Furthermore, 1,2-DCE proved effective as the PVK solvent in all-solution-processed QD-LEDs with an inverted structure where the QD EML is deposited prior to HTL formation. In this configuration, the QD EML remains vulnerable to damage during PVK deposition. Although 1,4-DO is typically used as the PVK solvent to minimize the corrosive effect on the QD layer,[26] we found that 1,2-DCE was even more effective at preventing this damage. As shown in Fig. S6,† UV-vis absorption spectra of QD films rinsed with various solvents, including CB, 1,4-DO, and 1,2-DCE, indicated that QD films rinsed with CB underwent a significant decrease in absorption intensity, while those rinsed with 1,4-DO showed approximately a 5% decrease. In contrast, QD films rinsed with 1,2-DCE displayed minimal change compared to unrinsed films. These findings confirm that 1,2-DCE is an optimal solution for PVK in all-solution-processed QD-LEDs, effective in both normal and inverted device architectures.

4. Conclusion

This study presents an effective strategy for fabricating TFB/PVK D-HTLs that significantly improve the performance of all-solution-processed QD-LEDs. We found that 1,2-DCE is a superior solvent to 1,4-DO for D-HTLs fabrication because it exhibits a lower dissolution rate of the underlying TFB layer. Analysis of the current–voltage characteristics of HODs, supported by power-law fitting, confirms that devices with 1,2-DCE-based D-HTLs exhibit enhanced hole injection efficiency within the QD EML. Furthermore, QD-LEDs employing TFB/PVK D-HTLs processed with 1,2-DCE achieved a maximum EQE of 13.7%—1.5 times greater than those of control devices with a single TFB

HTL and higher than those of D-HTL devices fabricated with 1,4-DO. These findings offer a practical approach to enhancing all-solution-processed QD-LEDs and provide a framework for improving hole injection and transport in the QD EML of solution-processed optoelectronic devices, thereby advancing overall device performance.

Data availability

The data that support the findings of this study are available from the corresponding author upon reasonable request.

Conflicts of interest

All authors declare no conflicts of interest.

Acknowledgements

References

1 M. Schlamp, X. Peng and A.-l. Alivisatos, *J. Appl. Phys.*, 1997, **82**, 5837–5842.

2 S.-Y. Yoon, J.-N. Han, Y.-J. Lee, A. I. Channa, D.-Y. Jo, H.-M. Kim, Y. Kim, S. M. Park, S. Park and Y.-H. Kim, *ACS Energy Lett.*, 2023, **8**, 1131–1140.

3 P. Liu, Y. Lou, S. Ding, W. Zhang, Z. Wu, H. Yang, B. Xu, K. Wang and X. W. Sun, *Adv. Funct. Mater.*, 2021, **31**, 2008453.

4 W. K. Bae, L. A. Padilha, Y.-S. Park, H. McDaniel, I. Robel, J. M. Pietryga and V. I. Klimov, *ACS Nano*, 2013, **7**, 3411–3419.

5 J. Lee, H. Jo, M. Choi, S. Park, J. Oh, K. Lee, Y. Bae, S. Rhee and J. Roh, *Small Methods*, 2024, 2301224.

6 J. Kim, J. Roh, M. Park and C. Lee, *Adv. Mater.*, 2024, **36**, 2212220.

7 V. L. Colvin, M. C. Schlamp and A. P. Alivisatos, *Nature*, 1994, **370**, 354–357.

8 S. Rhee, D. Hahm, H.-J. Seok, J. H. Chang, D. Jung, M. Park, E. Hwang, D. C. Lee, Y.-S. Park and H.-K. Kim, *ACS Nano*, 2021, **15**, 20332–20340.

9 X. Dai, Z. Zhang, Y. Jin, Y. Niu, H. Cao, X. Liang, L. Chen, J. Wang and X. Peng, *Nature*, 2014, **515**, 96–99.

10 Y. Yang, Y. Zheng, W. Cao, A. Titov, J. Hyvonen, J. R. Manders, J. Xue, P. H. Holloway and L. Qian, *Nat. Photonics*, 2015, **9**, 259–266.

11 H. Shen, Q. Gao, Y. Zhang, Y. Lin, Q. Lin, Z. Li, L. Chen, Z. Zeng, X. Li, Y. Jia, S. Wang, Z. Du, L. S. Li and Z. Zhang, *Nat. Photonics*, 2019, **13**, 192–197.

12 J. Kwak, W. K. Bae, D. Lee, I. Park, J. Lim, M. Park, H. Cho, H. Woo, D. Y. Yoon, K. Char, S. Lee and C. Lee, *Nano Lett.*, 2012, **12**, 2362–2366.

13 L. Qian, Y. Zheng, J. Xue and P. H. Holloway, *Nat. Photonics*, 2011, **5**, 543–548.

14 W. K. Bae, Y.-S. Park, J. Lim, D. Lee, L. A. Padilha, H. McDaniel, I. Robel, C. Lee, J. M. Pietryga and V. I. Klimov, *Nat. Commun.*, 2013, **4**, 2661.

15 S. Rhee, B. G. Jeong, M. Choi, J. Lee, W. H. Jung, J. Lim and J. Roh, *ACS Photonics*, 2023, **10**, 500–507.

16 F. Wang, W. Sun, P. Liu, Z. Wang, J. Zhang, J. Wei, Y. Li, T. Hayat, A. Alsaedi and Z. a. Tan, *J. Phys. Chem. Lett.*, 2019, **10**, 960–965.

17 X. Xiao, K. Wang, T. Ye, R. Cai, Z. Ren, D. Wu, X. Qu, J. Sun, S. Ding, X. W. Sun and W. C. H. Choy, *Commun. Mater.*, 2020, **1**, 81.

18 L. Zheng, G. Zhai, Y. Zhang, X. Jin, L. Gao, Z. Yun, Y. Miao, H. Wang, Y. Wu and B. Xu, *Superlattices Microstruct.*, 2020, **140**, 106460.

19 W. Zheng, D. Song, S. Zhao, B. Qiao, Z. Xu, J. Chen, P. Wang and Y. Liang, *Org. Electron.*, 2020, **77**, 105544.

20 Y. Sun, Y. Jiang, X. W. Sun, S. Zhang and S. Chen, *Chem. Rec.*, 2019, **19**, 1729–1752.

21 Y.-H. Won, O. Cho, T. Kim, D.-Y. Chung, T. Kim, H. Chung, H. Jang, J. Lee, D. Kim and E. Jang, *Nature*, 2019, **575**, 634–638.

22 S. Rhee, J. H. Chang, D. Hahm, B. G. Jeong, J. Kim, H. Lee, J. Lim, E. Hwang, J. Kwak and W. K. Bae, *ACS Nano*, 2020, **14**, 17496–17504.

23 Y.-Q.-Q. Yi, D. Qi, H. Wei, L. Xie, Y. Chen, J. Yang, Z. Hu, Y. Liu, X. Meng, W. Su and Z. Cui, *ACS Appl. Mater. Interfaces*, 2022, **14**, 39149–39158.

24 Y. Hwang, H. Jung, J. Kim, J. Park, A. Maheshwaran, B. Kang and Y. Lee, *ACS Appl. Mater. Interfaces*, 2025, **17**, 6668–6678.

25 X. Xiong, C. Wei, L. Xie, M. Chen, P. Tang, W. Shen, Z. Deng, X. Li, Y. Duan and W. Su, *Org. Electron.*, 2019, **73**, 247–254.

26 Y. Liu, C. Jiang, C. Song, J. Wang, L. Mu, Z. He, Z. Zhong, Y. Cun, C. Mai, J. Wang, J. Peng and Y. Cao, *ACS Nano*, 2018, **12**, 1564–1570.

27 L. z. Borg, D. Lee, J. Lim, W. K. Bae, M. Park, S. Lee, C. Lee, K. Char and R. Zentel, *J. Mater. Chem. C*, 2013, **1**, 1722–1726.

28 P.-L. T. Boudreault, N. Blouin and M. Leclerc, in *Polyfluorenes*, ed. U. Scherf and D. Neher, Springer Berlin Heidelberg, Berlin, Heidelberg, 2008, pp. 99–124, DOI: **10.1007/12_2008_139**.

29 J. Pan, J. Chen, Q. Huang, L. Wang and W. Lei, *RSC Adv.*, 2017, **7**, 43366–43372.

30 M. Auer-Berger, R. Trattnig, T. Qin, R. Schlesinger, M. V. Nardi, G. Ligorio, C. Christodoulou, N. Koch, M. Baumgarten and K. Müllen, *Org. Electron.*, 2016, **35**, 164–170.

31 Y.-L. Shi, F. Liang, Y. Hu, X.-D. Wang, Z.-K. Wang and L.-S. Liao, *J. Mater. Chem. C*, 2017, **5**, 5372–5377.

32 L. Lan, B. Liu, H. Tao, J. Zou, C. Jiang, M. Xu, L. Wang, J. Peng and Y. Cao, *J. Mater. Chem. C*, 2019, **7**, 5755–5763.

33 J. Chen, D. Song, S. Zhao, B. Qiao, W. Zheng and Z. Xu, *Org. Electron.*, 2021, **94**, 106169.

34 T.-H. Kim, K.-S. Cho, E. K. Lee, S. J. Lee, J. Chae, J. W. Kim, D. H. Kim, J.-Y. Kwon, G. Amaratunga, S. Y. Lee, B. L. Choi, Y. Kuk, J. M. Kim and K. Kim, *Nat. Photonics*, 2011, **5**, 176–182.

35 P.-C. Chiu and S.-H. Yang, *Nanoscale Adv.*, 2020, **2**, 401–407.

36 H. Feng, Y. Yu, G. Tang, S. Liu, L. Zhang and W. Xie, *J. Lumin.*, 2021, **231**, 117785.